Acta Cryst. (1997). D53, 524–534

Growth Mechanism of the (110) Face of Tetragonal Lysozyme Crystals

ARUNAN NADARAJAH,[a]*† MEIRONG LI[a]† AND MARC L. PUSEY[b]

[a]*Department of Chemical and Materials Engineering, University of Alabama in Huntsville, Huntsville, Alabama 35899, USA, and* [b]*Biophysics Branch ES76, NASA/Marshall Space Flight Center, Huntsville, Alabama 35812, USA. E-mail: anadaraj@eng.utoledo.edu*

(Received 21 October 1996; accepted 20 February 1997)

Abstract

The measured macroscopic growth rates of the (110) face of tetragonal lysozyme show an unexpectedly complex dependence on the supersaturation. In earlier studies it has been shown that an aggregate growth unit could account for experimental growth-rate trends. In particular molecular packing and interactions in the growth of the crystal were favored by completion of the helices along the 4_3 axes. In this study the molecular orientations of the possible growth units and the molecular growth mechanism were identified. This indicated that growth was a two-step process: aggregate growth units corresponding to the 4_3 helix are first formed in the bulk solution by stronger intermolecular bonds and then attached to the crystal face by weaker bonds. A more comprehensive analysis of the measured (110) growth rates was also undertaken. They were compared with the predicted growth rates from several dislocation and two-dimensional nucleation growth models, employing tetramer and octamer growth units in polydisperse solutions and monomer units in monodisperse solutions. The calculations consistently showed that the measured growth rates followed the expected model relations with octamer growth units, in agreement with the predictions from the molecular level analyses.

1. Introduction

Recent studies employing electron and atomic force microscopy (AFM) and Michelson interferometry have strikingly revealed the similarities in growth mechanisms between tetragonal lysozyme crystals and crystals of small-molecule materials (Durbin & Feher, 1990; Durbin & Carlson, 1992; Monaco & Rosenberger, 1993; Konnert, D'Antonio & Ward, 1994; Vekilov, Ataka & Katsura, 1995; Vekilov & Rosenberger, 1996). Faceted growth of these crystals was shown to occur by screw dislocation growth at lower supersaturations and by two-dimensional nucleation at higher supersaturations. These studies lead one to expect the growth rates to follow the same functional dependencies on supersaturation observed in small-molecule crystals. However, the measured lysozyme crystal growth rates show some unexpected trends with the supersaturation (Vekilov, Ataka & Katsura, 1995; Vekilov & Rosenberger, 1996; Nadarajah, Forsythe & Pusey, 1995).

Depending on the material and the growth conditions, the growth rates of small-molecule crystal faces can have a variety of functional dependencies on the supersaturation. For dislocation growth alone there are at least three functional forms: growth by isolated hillocks, growth by interacting hillocks and growth by complex sources (Chernov, 1984, 1988). Growth-rate models with various dependencies on the supersaturation exist for two-dimensional nucleation growth as well (Chernov, 1984; Boistelle & Astier, 1988). Tetragonal lysozyme crystal growth rates do not seem to follow the functional dependencies on supersaturation expected from any of these models. The growth rates display a more complex dependence, decaying asymptotically to zero when the supersaturation is lowered to zero and increasing rapidly when the supersaturation is increased (Vekilov, Ataka & Katsura, 1995; Vekilov & Rosenberger, 1996; Nadarajah, Forsythe & Pusey, 1995). When supersaturations are increased still further the growth rates attain a maximum before starting to decrease (Nadarajah, Forsythe & Pusey, 1995).

Some investigators have attributed these deviations in tetragonal lysozyme growth behaviour to the presence of impurities in the growth solution (Vekilov, Ataka & Katsura, 1995; Vekilov & Rosenberger, 1996). However, growth-rate trends for the (110) face were not altered even when highly purified lysozyme was employed for crystal growth rate measurements (Nadarajah, Forsythe & Pusey, 1995). We had suggested that these unusual growth-rate trends could be explained by the traditional models if the growth unit of the crystal was assumed to be a lysozyme aggregate instead of the monomer (Nadarajah, Forsythe & Pusey, 1995). In subsequent calculations we estimated the distribution of aggregates in lysozyme solutions under growth conditions, assumed that one of these aggregates was the growth unit for the (110) face, and that growth

† Current address: Department of Chemical and Environmental Engineering, University of Toledo, Toledo, OH 43606, USA.

occurred by one of the dislocation growth mechanisms (Li, Nadarajah & Pusey, 1995). The enthalpies of aggregation were determined from data fits with the experimentally measured growth rates. The predicted growth rates and their trends with temperature for octamer units agreed remarkably well with the experimental data, while predicted enthalpies for the formation of octamers were close to those obtained from the solubility data (Li, Nadarajah & Pusey, 1995). These results suggested that, at least for the (110) face of tetragonal lysozyme, growth occurred by the addition of octamer growth units.

Such macroscopic analyses cannot identify the overall shape or the orientation of the molecules that make up such an octamer, or why crystal growth should proceed by octamer addition. However, our recent analysis of the molecular packing arrangement of the tetragonal lysozyme indicated that the crystals consisted of molecules in strongly bonded helices along the 4_3 crystallographic axes (Nadarajah & Pusey, 1996). These strongly bonded helices are attached to each other by weaker bonds, completing the crystal packing arrangement. This suggests that there is a preferential pathway for the growth of this crystal, with growth proceeding by the formation of the 4_3 helices. This prediction was confirmed by high-resolution AFM scans of the (110) face, which showed that the molecular arrangements on these faces corresponded to complete 4_3 helices (Konnert, D'Antonio & Ward, 1994).

The above studies of the growth mechanism of tetragonal lysozyme at the molecular level can now be used to identify the orientations of molecules in the aggregate growth unit formed in solution, for the (110) face. Additionally, since the relative magnitudes of all the intermolecular bonds in the crystal are now known from our earlier study (Nadarajah & Pusey, 1996), the likely crystallization pathway can be deduced by assuming the stronger bonds are formed before the weaker ones. We will attempt to achieve both of these goals in this study. A drawback of our earlier analysis of the macroscopic growth rates of the (110) faces was that only one dislocation growth mechanism was considered (Li, Nadarajah & Pusey, 1995). In this study a more comprehensive analysis will be undertaken, with other possible dislocation and two-dimensional nucleation growth mechanisms investigated.

2. Molecular growth mechanism and growth unit structure

The construction of the tetragonal lysozyme crystal model involved suitably assembling molecules with the eight unique orientations in the unit cell for the space group $P4_32_12$ (*International Tables for Crystallography*, 1983; Diamond, 1974). Fig. 1(*a*) shows the unit cell viewed along the *c* crystallographic axis, with the reference molecule labeled *M* and the other seven molecules labeled *A* to *G*, employing a simplified representation for each molecule with the location of the active site clearly shown (Nadarajah & Pusey, 1996). The space occupied by each lysozyme molecule in the crystal (the asymmetric unit) is a rectangular block of dimensions 28.0 × 28.0 × 37.9 Å as shown in Fig. 1(*b*). This rectangular block of Fig. 1(*b*) and the simplified

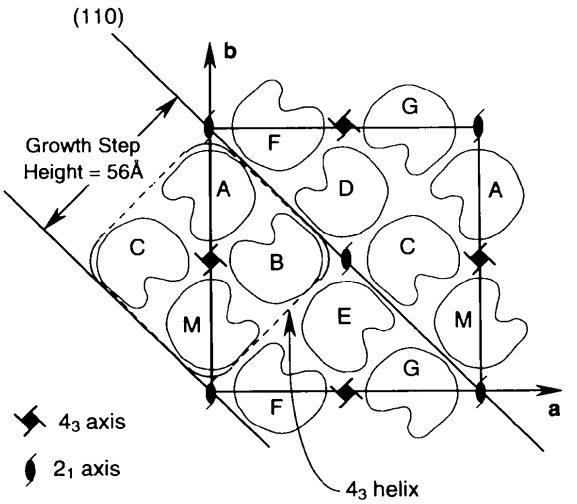

(*a*)

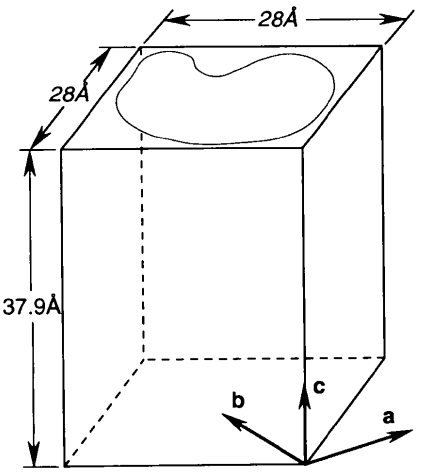

(*b*)

Fig. 1. Simplified representations of crystalline lysozyme molecules. (*a*) The unit cell of tetragonal lysozyme (space group $P4_32_12$), employing a simplified shape for each molecule, with the reference molecule labelled *M* and the other seven orientations labelled *A* to *G*. The four molecules that form a single turn of the 4_3 helix and the diagonal lines corresponding to the (110) faces are also shown. (*b*) The space occupied by the reference molecule *M* in the tetragonal form, which can also be used to represent individual lysozyme molecules.

Table 1. *The total number of interatomic bonds that constitute each molecular interaction in tetragonal lysozyme crystals*

These numbers are indicative of the relative strengths of the interactions. The breakdown of this total of inter-atomic bonds into types, such as hydrogen bonds and salt bridges, are given elsewhere (Nadarajah & Pusey, 1996).

Interaction	Number of bonds
V	1
W	10
X	10
Y	33
Z	22

representation of Fig. 1(*a*) will be used to represent lysozyme molecules in subsequent constructions.

Fig. 1(*a*) also indicates the 4_3 helix which was shown to be the dominant structure in the internal molecular packing arrangement of tetragonal lysozyme (Nadarajah & Pusey, 1996). This is primarily because of the strong set of intermolecular bonds (*W* and *Z*) holding this helix together (see Table 1). These are shown in Fig. 2 along with the weaker set of bonds (*X* and *Y*) which bind the helices to each other. Each molecule in the helix is bound to another one with two *W* bonds to two molecules displaced $\frac{1}{4}$ turn and by two *Z* bonds with two other molecules displaced by $\frac{3}{4}$ turn of the helix.

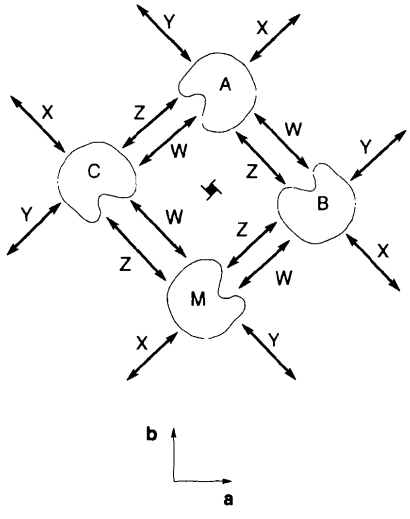

Fig. 2. The nearest neighbor interactions between the molecules forming the 4_3 helix. Each interaction is comprised of several electrostatic, hydrogen and hydrophobic bonds between individual atoms (Nadarajah & Pusey, 1996). Each molecule in the *M–C–A–B* sequence is displaced along the *c* axis by a $\frac{1}{4}$ turn of the helix, with respect to the previous molecule. Two *Z* interactions bind each molecule to one a $\frac{1}{4}$ turn above and to one a $\frac{1}{4}$ turn below it, while two *W* interactions bind each molecule to one a $\frac{3}{4}$ turn above and one a $\frac{3}{4}$ turn below it. The molecules of each 4_3 helix are bound to those in neighboring helices by one *X* and one *Y* interaction on each of the four sides.

From this structure of tetragonal lysozyme, it should be clear that growth steps on the (110) face will correspond to the 4_3 helix as indicated in Fig. 1(*a*) (Nadarajah & Pusey, 1996). This has been confirmed by AFM studies which showed that all growth steps on this face were 56 Å or bimolecular in height and that the face always corresponded to the plane containing the 2_1 axes (Konnert, D'Antonio & Ward, 1994). Thus, any growth unit for this face must at least be a dimer, otherwise monomolecular steps and planes containing the 4_3 axes would have been seen on this face. With a dimer growth unit it may be possible to obtain bimolecular steps (Fig. 3*a*). However, because of the regularity and symmetry of the 4_3 helix, it is equally possible to obtain monomolecular steps as well with a dimer growth unit, as shown in Fig. 3(*b*). Thus, such a growth unit would have resulted in nearly half the growth steps being monomolecular, contrary to experimental observations. The growth unit must at least be a 4_3 tetramer to ensure continuous growth by bimolecular steps, as shown by Fig. 3(*c*). We can conclude that the growth unit for the (110) face must be this tetramer or a larger aggregate.

Nucleating a tetramer on a growth step of the (110) face is equivalent to a four-molecular reaction. This is an unlikely event even for spherically symmetric small molecules, and more so for large, non-symmetric protein molecules with precise orientation requirements. Thus, these growth units must be formed in solution by sequential, bimolecular reactions (Fig. 3). The reason for growth to proceed in this manner for tetragonal lysozyme faces is suggested by the imbalance in the strengths of the bond sets *W–Z* and *X–Y*. Formation of the weaker *X–Y* bond set is the rate-limiting step in the growth of the crystal faces. This leads to the rapid formation and accumulation in solution of the aggregates corresponding to the 4_3 helices by the stronger *W–Z* bond set, followed by slow attachment of the growth units to the crystal face by the weaker *X–Y* bond set. This can be expressed by the following

$$\text{monomer} \xrightarrow[\text{formation}]{W\text{–}Z\text{ bond}} \text{growth unit} \xrightarrow[\text{formation}]{X\text{–}Y\text{ bond}} \text{crystal.}$$

Moreover, this means that the attachment of the growth unit to the crystal, that is the crystal growth rate, becomes the rate-determining step. This also means that the relatively rapid and reversible aggregation reactions in solution will all be at equilibrium during crystal growth.

The above sequence of events have been shown to occur as well by numerous studies of lysozyme aggregation in solution. In several of these studies the focus was on measuring the aggregate distribution employing a variety of techniques, including ultracentrifugation (Sophianopoulos & Van Holde, 1964;

Behlke & Knespel, 1996), light scattering (Pusey, 1991), and neutron scattering (Boué, Lefaucheux, Robert & Rosenman, 1993). They all showed that with increasing lysozyme concentration the average particle size of the solute increased steadily, with sizes corresponding to those of octamers and larger aggregates at crystallization conditions. The recent work of Minezaki, Nimura, Ataka & Katsura (1996), employing neutron scattering, showed the formation of higher order lysozyme aggregates with molecular interactions in solution taken into account. Of particular interest are studies where the enzymatic activity of lysozyme was followed (Wilcox & Daniel, 1954; Sophianopoulos, 1969; Zehavi & Lustig, 1971; Studebaker, Sykes & Wien, 1971; Banerjee, Poglotti & Rupley, 1975; Hampe, Tondo & Hasson-Voloch, 1982). They showed that the activity progressively decreased with increasing lysozyme concentration in solution. This indicated not only that aggregation was occurring, but also that they corresponded to the 4_3 helix (Nadarajah & Pusey, 1996). Such aggregation would produce the decreases in the activity from the progressive blocking of the lysozyme active sites as the 4_3 helix is formed (Fig. 3). In our recent work we measured the aggregate distributions of lysozyme solutions with a dialysis technique and compared them with the distributions deduced from the growth kinetics of lysozyme crystals for the mechanism shown in Fig. 3 (Wilson, Adcock-Downey & Pusey, 1996). The two aggregate distributions agreed remarkably well.

The above results make it clear that the growth unit must be at least a tetramer formed in the bulk solution corresponding to the 4_3 helix. However, the aggregation process will not end with the formation of the tetramer, as still larger aggregates can be formed by the same strong *W–Z* bond set. Fig. 4(*a*) shows the 4_3 tetramer constructed employing the rectangular blocks of Fig. 1(*b*) to represent each lysozyme molecule, while Fig. 4(*b*) shows a 4_3 hexamer and Fig. 4(*c*) a 4_3 octamer. Much larger 4_3 aggregates are likely to be formed only in lower proportions as their length makes them mechanically unstable. They will either break up into smaller units or form larger ones which become nucleii. This leaves the possibility that at least one or more of the aggregates shown in Fig. 4 could be the growth unit(s).

Screw dislocation hillocks and two-dimensional nucleation islands on the (110) face of tetragonal lysozyme both display a pronounced anisotropy (Durbin & Feher, 1990; Durbin & Carlson, 1992; Konnert, D'Antonio & Ward, 1994). They are more elongated in the [$\bar{1}$10] direction than in the [001] direction. Moreover, etching studies have shown that etch pits on this face display the same anisotropy, with greater elongation of the etch pits in the [$\bar{1}$10] direction (Monaco & Rosenberger, 1993). This suggests that the growth unit for this face may be a larger aggregate, such as an octamer, rather than a smaller one, such as a tetramer. As discussed below, this is based on the different number of bonds formed when each unit is incorporated into the crystal. Depending on the attachment site, tetramer units can form up to four *X–Y* and two *W–Z* bond sets (Fig. 5*a*), while octamers may form as many as eight *X–Y* and two *W–Z* bond sets (Fig. 5*b*).

Fig. 6(*a*) shows a growth island formed by tetramer and octamer units. For a tetramer unit, the [001] direction will be preferred for addition to this island as this will involve the formation of one *W–Z* and one *X–Y*

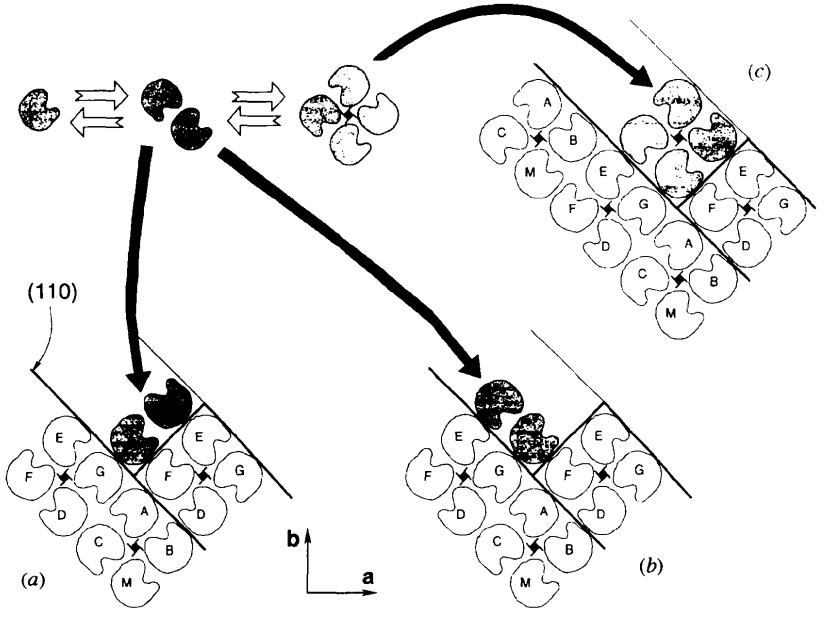

Fig. 3. Possible ways for the growth of a bimolecular growth step on the (110) face. Case (*a*) shows that this can be accomplished by the addition of dimers from the bulk solution, but given the symmetry of the 4_3 helix, these same dimers can also form monomolecular steps as shown by case (*b*). To ensure that growth proceeds exclusively by bimolecular steps, as observed experimentally, at least a tetramer growth unit is needed as shown by case (*c*).

bond set. Attachment in the [$\bar{1}$10] direction will involve two *X–Y* bond sets. For octamers attachment in the [001] direction will involve one *W–Z* and two *X–Y* bond sets, while in the [$\bar{1}$10] direction four *X–Y* bond sets will be formed. Since the magnitude of two *X–Y* bond sets exceeds that of one *W–Z* bond set (Nadarajah & Pusey, 1996), for octamers the [$\bar{1}$10] direction will be the preferred one for growth as has been experimentally observed (Durbin & Feher, 1990; Durbin & Carlson, 1992; Konnert, D'Antonio & Ward, 1994).

Fig. 6(*b*) shows an etch pit on the (110) face. The removal of a tetramer unit from the side wall in the [001] direction during dissolution will involve breaking one *W–Z* and three *X–Y* bond sets, while for dissolution in the [$\bar{1}$10] direction two *W–Z* and two *X–Y* bond sets must be broken. Removal of octamer units requires breaking one *W–Z* and six *X–Y* bond sets in the [001] direction and only two *W–Z* and four *X–Y* bond sets in the [$\bar{1}$10] direction. Once again for octamer units the etching will be preferentially in the [$\bar{1}$10] direction as observed experimentally (Monaco & Rosenberger, 1993), while for tetramer units it would be in the [001] direction. We can conclude that both growth and dissolution processes proceed largely by octamer units. However, it is possible that some growth and dissolution on the (110) face can proceed by other growth units: by larger 4_3 aggregates in the [$\bar{1}$10] direction and by tetramers in the [001] direction.

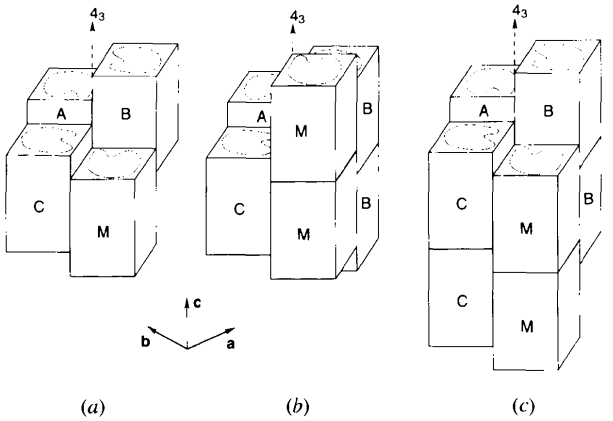

(*a*) (*b*) (*c*)

Fig. 4. Possible aggregate growth units corresponding to the 4_3 helix: (*a*) tetramer, (*b*) hexamer and (*c*) octamer.

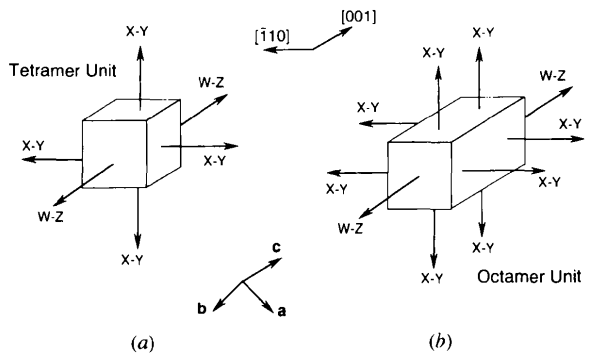

(*a*) (*b*)

Fig. 5. Simplified representations of (*a*) a tetramer and (*b*) an octamer unit, showing the interactions that can occur when they attach to the (110) face.

3. Growth-rate models

From the arguments presented in the previous section the lysozyme aggregation process in the solution can be considered to be at equilibrium relative to the rate of growth-unit attachment to the crystal. Thus, a decrease in the solution temperature or an increase in the protein concentration would result in a corresponding increase in the equilibrium concentrations of the higher order aggregates. Most of the work in modelling lysozyme aggregation has been confined to measurements done at pH values above 5.0 (Sophianopoulos & Van Holde, 1964; Sophianopoulos, 1969; Hampe, Tondo & Hasson-Voloch, 1982). At the lower pH values customarily employed for tetragonal lysozyme crystal growth, the near absence of equilibrium constants for the aggregation process means that they must be estimated as part of the growth-rate model.

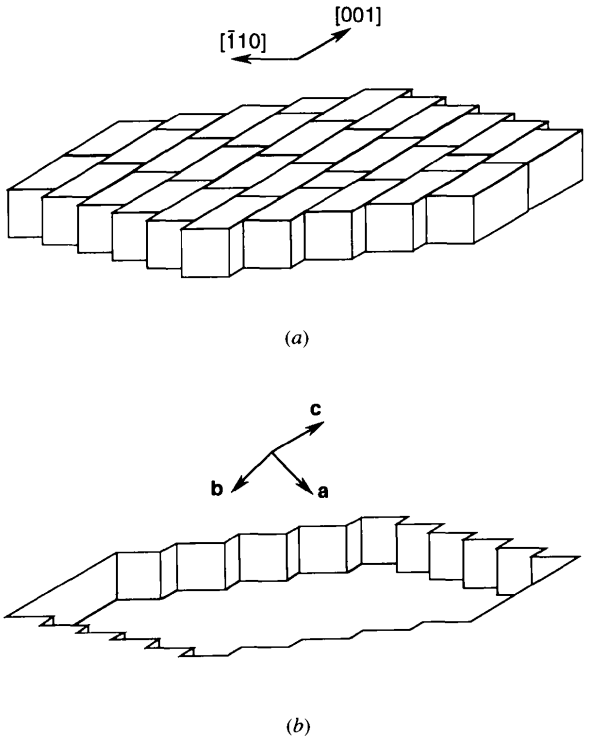

(*a*)

(*b*)

Fig. 6. Representations of (*a*) a growth island and (*b*) an etch pit on the (110) face, employing the 4_3 tetramers and octamers shown in Fig. 5. Both are drawn to indicate the anisotropies in the [$\bar{1}$10] and [001] directions, observed experimentally.

The equilibrium process to form the aggregate units discussed in the previous section can be represented by a series of reversible, bimolecular aggregation reactions given by,

$$\text{monomer} \rightleftharpoons \text{dimer} \rightleftharpoons \text{tetramer} \rightleftharpoons \text{octamer} \rightleftharpoons \text{higher order aggregates.}$$

The choice of 4_3 aggregate species in the above needs some justification. The omission of trimers in this equation can be readily explained. They are less stable than dimers, because they have a more unwieldy shape which is not stabilized with additional bonds. Unlike tetramers they do not form a securely bonded complete turn of the 4_3 helix. This reduced stability of trimers will translate to extremely small equilibrium concentrations compared with dimers and tetramers. However, unlike for trimers, it is harder to justify omitting aggregates larger than a tetramer, such as hexamers. They have been omitted here for ease of calculation, but are likely to be present in significant numbers in lysozyme solutions under crystal growth conditions.

Equilibrium constants can be defined for the above series of reactions. For the formation of $2i$-mers from i-mers the equilibrium constant $K_{i\to 2i}$ is given by,

$$K_{i\to 2i} = K^0_{i\to 2i} \exp(\Delta H_{i\to 2i}/RT) = (C_{2i}^{1/2}/C_i)^{1/i}, \quad (1)$$

where C_i is the i-mer concentration, T is the temperature, $K^0_{i\to 2i}$ is the pre-exponential constant and $\Delta H_{i\to 2i}$ is the heat of reaction, with all variables defined on the basis of per mole of monomeric lysozyme. The enthalpies and the pre-exponential constants were determined from data fits to the measured growth rates in our earlier calculation, assuming a dislocation growth model (Li, Nadarajah & Pusey, 1995). The results agreed well with the enthalpies estimated from the solubility data (Cacioppo & Pusey, 1991), and earlier estimates of the equilibrium constant for the formation of dimers (Wilson, Adcock-Downey & Pusey, 1996). These values of the equilibrium constants and enthalpies will be utilized herein to determine the aggregate distributions in solution.

The growth rate R of a dislocation hillock is given by,

$$R = pv, \quad (2)$$

where p is the hillock slope and v is the tangential growth-step velocity given by,

$$v = \beta\Omega(C - S), \quad (3)$$

where C is the solute concentration, S is the solubility at that temperature, β is the kinetic coefficient and Ω is the volume occupied by the growth unit in the crystal (Chernov, 1984, 1988). Although v remains the same, the functional form of the slope can change depending on the growth conditions. For isolated growth hillocks p is given by

$$p = hkT\sigma/19\Omega\alpha, \quad (4)$$

where h is the growth-step height, T the temperature, σ the supersaturation, defined by $\ln C/S$, and α is the step free energy. In small-molecule crystals, for faces with several adjacent dislocation sources and strong diffusional interaction between the steps, the hillock slope was found to remain essentially constant (Vekilov & Kuznetsov, 1992). This has also been shown to be the case for the (101) face of tetragonal lysozyme over a relatively wide range of supersaturations (Vekilov, Ataka & Katsura, 1995). Thus, this case merits consideration here, and p in (2) reduces to a constant. Finally for the case of complex dislocation sources, of a Burger's vector magnitude mh, the slope is given by

$$p = \frac{mhkT\sigma}{19\Omega\alpha + 2LkT\sigma}, \quad (5)$$

where L is the perimeter of the complex source.

For two-dimensional nucleation the commonly used model of the growth rate is given by (Chernov, 1984, 1988),

$$R = \text{const. } C^{1/3}\sigma^{1/6}(C - S)^{2/3} \exp(-\pi h\Omega\alpha^2/3k^2T^2\sigma). \quad (6)$$

Although other mechanisms have been suggested (Durbin & Feher, 1990; Boistelle & Astier, 1988), they are rarely employed. Given its widespread use in crystal growth studies, only the above model will be considered here for two-dimensional nucleation growth. As written, (2)–(6) are valid only for monomer growth from monodisperse solutions. For aggregate growth on the (110) face of tetragonal lysozyme they will have to be modified, with C, S and σ being replaced by C_n, S_n and σ_n. Here C_n is the n-mer growth-unit concentration in the nutrient solution, S_n is the concentration of that n-mer at saturation and σ_n is the n-mer supersaturation defined by $\ln C_n/S_n$. Some of the parameters, such as Ω, will have to be modified as well for n-mer growth.

In assessing the above models, comparisons were made with measured averaged growth rates of the (110) face at three sets of conditions: pH 4.0/5% NaCl, pH 4.6/3% NaCl, and pH 5.0/5% NaCl (Nadarajah, Forsythe & Pusey, 1995). At each lysozyme concentration and temperature the distribution of aggregates was determined as described previously (Li, Nadarajah & Pusey, 1995). The values of the equilibrium constants and enthalpies used in the calculation were taken from the earlier study, and are listed here in Table 2. Growth of the (110) face by three different growth units were considered: monomers, tetramers and octamers. The measured growth rates were plotted against the various functional relationships given by the monomer (monodisperse), tetramer and octamer versions of (2)–(6).

Table 2. *Values of the parameters in (1) used for calculating the distribution of aggregates in lysozyme solutions*

The values were taken from the work of Li, Nadarajah & Pusey (1995).

Parameter/Condition	pH 4.6, 3% NaCl	pH 4.0, 5% NaCl	pH 5.0, 5% NaCl
$K^0_{1\to2}$ ($M^{-1/2}$)	4.7×10^{-6}	8.7×10^{-6}	4.4×10^{-3}
$K^0_{2\to4}$ ($M^{-1/4}$)	1.5×10^{-4}	1.3×10^{-3}	7.0×10^{-3}
$K^0_{4\to8}$ ($M^{-1/8}$)	6.7×10^{-3}	1.1×10^{-2}	1.4×10^{-2}
$K^0_{8\to16}$ ($M^{-1/16}$)	5.6×10^{-2}	6.0×10^{-2}	5.9×10^{-2}
$\Delta H_{1\to2}$ (kJ mol^{-1})*	−37.7	−37.7	−20.9
$\Delta H_{2\to4}$ (kJ mol^{-1})	−25.1	−20.9	−16.7
$\Delta H_{4\to8}$ (kJ mol^{-1})	−14.2	−13.0	−12.6
$\Delta H_{8\to16}$ (kJ mol^{-1})	−7.9	−7.9	−9.2

* 1 kcal = 4.184 kJ.

4. Results

The measured (110) growth rates are plotted against $\sigma(C-S)T/T_{av}$ in Fig. 7(*a*), where T_{av} is the average temperature 286 K for the 277–295 K temperature range considered here and is used to normalize T. This corresponds to the functional relationship of the growth rate for dislocation-led growth by isolated hillocks in monodisperse systems given by (2)–(4). It is clear that the growth rates do not follow the functional relationship given by this equation. Figs. 7(*b*) and 7(*c*) show the same data plotted against $(C_4-S_4)\sigma_4 T/T_{av}$ and $(C_8-S_8)\sigma_8 T/T_{av}$. The tetramer versions of (2)–(4) produce poor agreement as well (Fig. 7*b*), and it is clear that the best fit is obtained with the octamer versions of the equations (Fig. 7*c*). Thus, growth by the isolated dislocation hillock mechanism agrees with the data closely for octamer growth units, but not for tetramer growth units and for growth from a monodisperse solution.

Fig. 8 is plotted for the case of adjacent interacting hillocks with constant slopes. In Fig. 8(*a*) the growth rate is plotted against $(C-S)$ and shows that the expected relationship with constant p in (2) is not followed. In Figs 8(*b*) and 8(*c*) the growth rate is plotted against (C_4-S_4) and (C_8-S_8). It is clear that the growth rates best follow the expected relationship for constant hillock slopes when the growth unit is assumed to be an octamer. For complex dislocation sources, (2), (3) and (5) may be rewritten as

$$\frac{T\sigma(C-S)}{R} = \frac{19\alpha}{mh\beta k} + \frac{2LT\sigma}{mh\beta\Omega}. \qquad (7)$$

In Fig. 9(*a*) the term $T\sigma(C-S)/T_{av}R$ is plotted against $T\sigma/T_{av}$, with a corresponding plot for octamers in Fig. 9(*b*). These figures show that the expected relationship is not followed for any of these cases.

For growth by two-dimensional nucleation (6) can be rewritten as,

$$\ln\left[\frac{R}{C^{1/3}\sigma^{1/6}(C-S)^{2/3}}\right] = \text{const} - \frac{qT_{av}^2}{T^2\sigma}, \qquad (8)$$

where q is the dimensionless ratio $\pi h\Omega\alpha^2/3k^2T_{av}^2$. For the three data sets the term $\ln[R/C^{1/3}\sigma^{1/6}(C-S)^{2/3}]$ on the left-hand side of (8) was plotted against $T_{av}^2/T^2\sigma$. Similar plots were generated for tetramer and octamer units. The slopes of these plots were obtained from

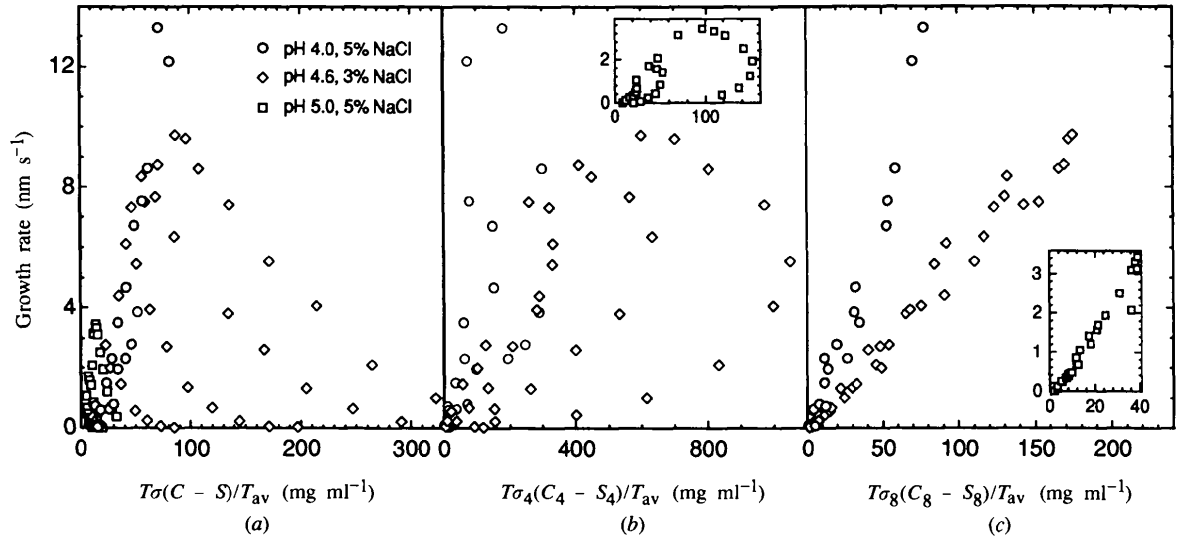

Fig. 7. Plots of the measured averaged growth rates of the (110) face of tetragonal lysozymes at three conditions for the functional relationship for dislocation growth by isolated hillocks given by (2), (3) and (4) against $T\sigma(C-S)/T_{av}$ for monomer growth from monodisperse solutions and against $T\sigma_4(C_4-S_4)/T_{av}$ and $T\sigma_8(C_8-S_8)/T_{av}$ for tetramer and octamer growth from polydisperse solutions. The insets show the plots for tetramer and octamer growth at the pH 5.0/5% NaCl condition on an expanded scale.

linear least-squares data fits, and they gave nine values of q. These values were then used to plot the growth rate against the term $C^{1/3}\sigma^{1/6}(C-S)^{2/3}\exp(-qT_{av}^2/T^2\sigma)$ in (6). These are shown in Fig. 10. They clearly indicate that the octamer growth model better displays the expected linear behaviour than the tetramer model or the monomer model.

5. Discussion

Comparing the dislocation growth mechanisms, Figs. 7(*a*), 8(*a*) and 9(*a*) show that the growth rates definitely do not follow these standard mechanisms if it is assumed that the nutrient solutions are monodisperse and growth occurs only by monomer addition. Clearly, another

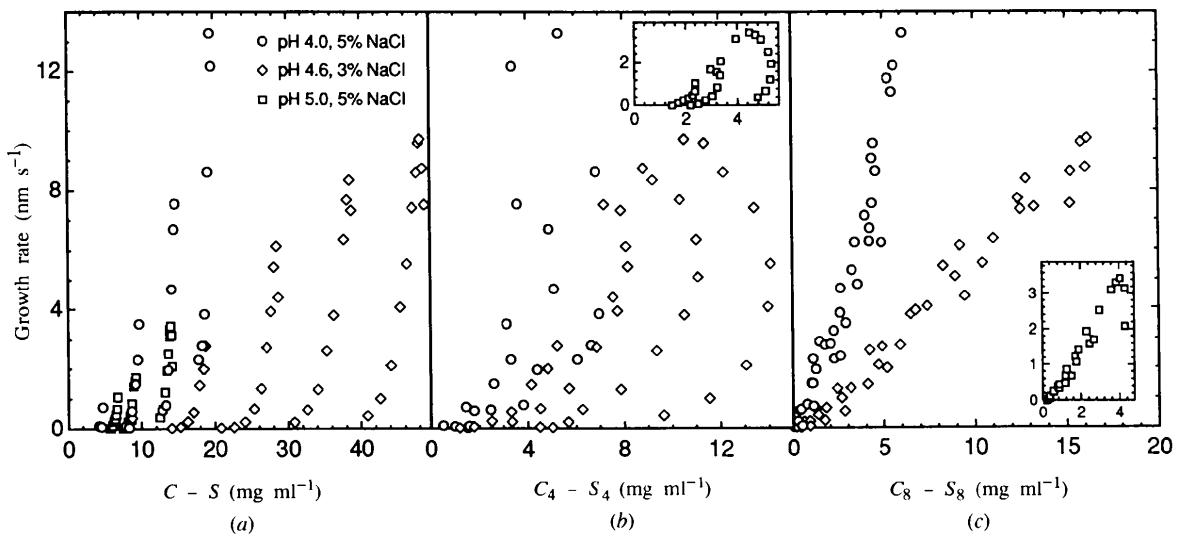

Fig. 8. Plots of the measured averaged growth rates of the (110) face of tetragonal lysozyme at three conditions for the functional relationship for dislocation growth by adjacent hillocks, given by (2) and (3) with constant hillock slope: against $(C-S)$ for monomer growth, against (C_4-S_4) for tetramer growth and against (C_8-S_8) for octamer growth. The insets show the plots for tetramer and octamer growth at the pH 5.0/5% NaCl condition on an expanded scale.

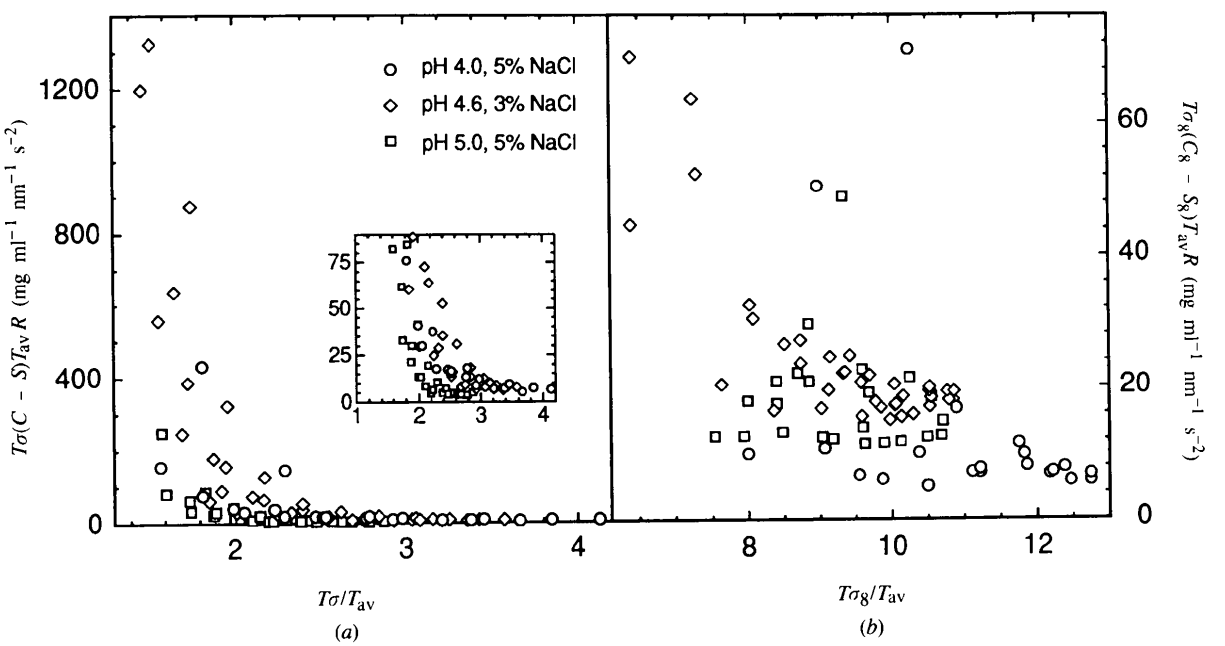

Fig. 9. Plots of the functional relationship for growth by complex dislocation sources in (7), employing the measured averaged growth rates of the (110) face of tetragonal lysozyme at three conditions: $T\sigma(C-S)/T_{av}R$ plotted against $T\sigma/T_{av}$ for monomer growth and $T\sigma_8(C_8-S_8)/T_{av}R$ plotted against $T\sigma_8/T_{av}$ for octamer growth. The inset shows the plot for monomer growth on an expanded scale at high supersaturations.

mechanism is needed to predict the observed growth-rate trends. Figs. 7(*b*) and 8(*b*) show that growth by tetramer addition, from a solution containing a distribution of aggregates, but this hardly improves the predictions. However, Figs. 7(*c*) and 8(*c*) show that dislocation growth by octamer addition can account for the measured growth trends quite well. A cursory comparison may indicate that there is little to distinguish the linearity of the data in Figs. 7(*c*) and (8*c*). [It should be noted here that a linear relationship between R and $C_8\sigma_8$ was assumed to imploy growth by interacting hillocks with constant slopes in our earlier study (Li, Nadarajah & Pusey, 1995), but as discussed in the previous sections and shown by (2), (3) and (4) and Fig. 7(*c*), this is more likely to imply growth by isolated hillocks.] A regression analysis of these two plots showed that growth by the isolated hillocks model provides a marginally better linear fit.

There could be at least two reasons for the apparent similarity of fits with these two dislocation growth mechanisms indicated by Figs. 7(*c*) and 8(*c*). First, the growth-rate data considered here are from macroscopic measurements, averaged over the entire (110) face (Nadarajah, Forsythe & Pusey, 1995). They may not be sensitive enough to distinguish between the microscopic or local growth mechanisms on that face. Second, these growth mechanisms differ principally in their functional relationships with the octamer supersaturation σ_8. Compared with that of C_8, the percentage variation of σ_8 with temperature is moderate and this is shown in Fig. 11. This variation is moderated further when σ_8 appears in equations multiplied by T or T^2. This may also partly account for the constant hillock slopes seen in earlier studies (Vekilov, Ataka & Katsura, 1995), as the term $T\sigma_8$ for octamers in (4) changes relatively little over the temperature and concentration range considered here.

This property of σ_8 has the effect of minimizing the influence of the attachment mechanism of the growth unit on the face growth rate. Thus, unlike small-molecule crystal growth from monodisperse solutions, dislocation-led growth-rate trends with temperature of lysozyme crystals show an independence from the attachment mechanism. However, these are strongly affected by the choice of the growth unit. Growth of the (110) face by octamer addition changes the growth-rate dependence on the supersaturation σ considerably from the expected values. This is shown by our earlier studies (Nadarajah, Forsythe & Pusey, 1995; Li, Nadarajah & Pusey, 1995), and by Figs. 7 and 8. This suggests that the averaged or macroscopic growth-rate measurements may be sensitive enough to show that lysozyme crystals grow by an aggregate growth unit, but may not be sensitive enough to identify the actual growth-unit attachment mechanism to the crystal face.

Figs. 9(*a*) and 9(*b*) indicate that the (110) face does not grow by complex dislocation sources. Assuming tetramer growth units also gave poor agreement (not shown). This agrees with microscopic studies which have not reported such sources (Durbin & Feher, 1990; Durbin & Carlson, 1992; Konnert, D'Antonio & Ward, 1994). Complex sources have been seen occasionally on tetragonal lysozyme crystal faces by atomic force microscopy but their occurrence is

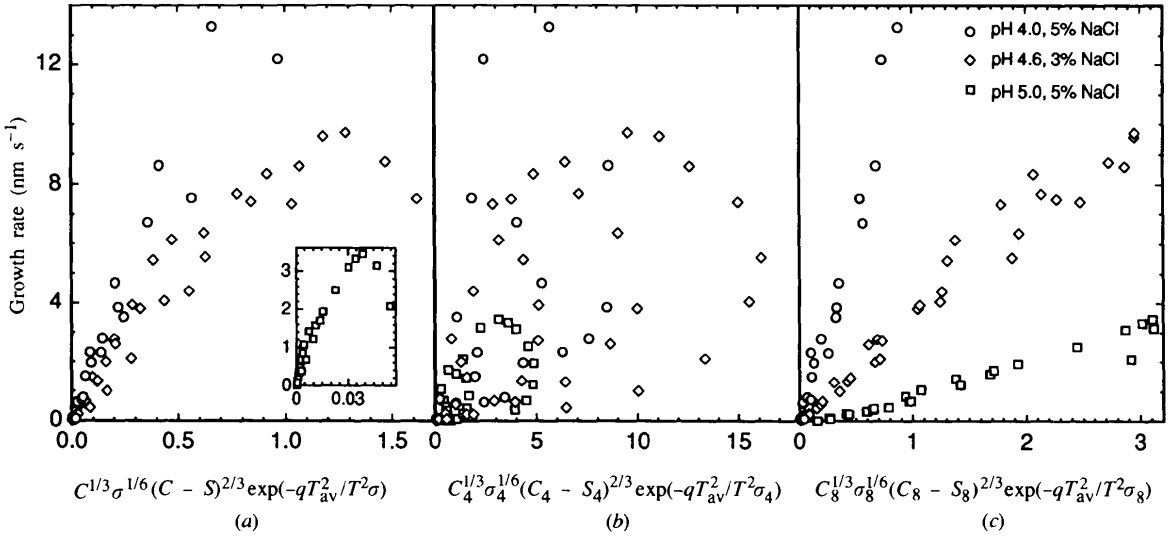

Fig. 10. Plots of the measured averaged growth rates of the (110) face of tetragonal lysozyme at three conditions for the functional relationship of two-dimensional nucleation growth given by (6): against $C^{1/3}\sigma^{1/6}(C-S)^{2/3}\exp(-qT_{av}^2/T^2\sigma)$ for monomer growth, against $C_4^{1/3}\sigma_4^{1/6}(C_4 - S_4)^{2/3}\exp(-qT_{av}^2/T^2\sigma_4)$ for tetramer growth and against $C_8^{1/3}\sigma_8^{1/6}(C_8 - S_8)^{2/3}\exp(-qT_{av}^2/T^2\sigma_8)$ for octamer growth. The inset shows the plot for monomer growth at the pH 5.0/5% NaCl condition on an expanded scale. The values of q are the slopes obtained by plotting $\ln R/C^{1/3}\sigma^{1/6}(C-S)^{2/3}]$ in (8) against $T_{av}^2/T^2\sigma$, for monomers, tetramers and octamers.

probably not frequent enough to cause the growth rates to follow the monomer or aggregate versions of (2), (3) and (5).

Although Figs. 7(*c*) and 8(*c*) seem to indicate that the two dislocation growth mechanisms are valid over the entire data range, a close examination clearly shows a gradual deviation from linearity with increasing concentrations and supersaturations. This most likely indicates the change in the growth-rate relationship from that corresponding to dislocation growth to growth by two-dimensional nucleation. In fact the properly linear regions in Figs. 7(*c*) and 8(*c*) are relatively small, near the origin. These results are in keeping with experimental observations on the (110) and (101) faces. These microscopic studies have indicated that growth occurs predominantly by dislocations only for $\sigma < 1.5$ and predominantly by two-dimensional nucleation for $\sigma > 2$ (Durbin & Feher, 1990; Durbin & Carlson, 1992; Monaco & Rosenberger, 1993; Konnert, D'Antonio & Ward, 1994; Vekilov, Ataka & Katsura, 1995; Vekilov & Rosenberger, 1996).

The above discussion suggests that most of the growth-rate data considered here should follow the two-dimensional nucleation growth mechanism. Comparisons of Figs. 10(*a*), 10(*b*) and 10(*c*) show that the two-dimensional nucleation model provides a somewhat better fit to the data for monomer growth from monodisperse solutions, than with any of the dislocation growth models considered above. However, this figure also shows that the two-dimensional nucleation model for monomer growth given by (6) seems to fit the growth-rate data best at low supersaturations where dislocation growth may be expected to prevail. At higher supersaturations the growth rates deviate from linearity significantly. This is the reverse of the expected trends from the model. This more than any other reason indicates that the two-dimensional nucleation model with monomer growth does not describe the observed growth-rate trends of tetragonal lysozyme. Fig. 10(*b*) shows that the data does not agree with a tetramer two-dimensional nucleation model either.

Fig. 10(*c*) shows the remarkable agreement of the growth rates with the two-dimensional nucleation model for octamer growth units given by (6). The agreement is particularly good at the higher supersaturations as expected from such a model. There is some deviation from linearity at low supersaturations. This, too, is in keeping with the expected deviation from predictions by a two-dimensional nucleation model in a dislocation growth regime. The determination of the values of q in (8) also allowed the step free energy α to be determined. Employing a step height of 56 Å for the (110) face (Fig. 1*a*), and eight times the volume occupied by a single molecule in tetragonal lysozyme crystals for Ω (Fig. 1*b*), the values of α obtained were: 0.58×10^{-3} J m^{-2} at pH 4.0, 5% NaCl, 0.50×10^{-3} J m^{-2} at pH 4.6, 3% NaCl and 0.26×10^{-3} J m^{-2} at pH 5.0, 5% NaCl. These values are much smaller than those encountered in small-molecule systems (Chernov, 1984, 1988).

The agreement of the growth-rate data with the two-dimensional nucleation model of (6) is shown even more clearly when the growth rates are plotted against the growth conditions. In Fig. 12 the growth-rate data set at pH 4.6, 3% NaCl is plotted against the temperature for various concentrations, along with the model predictions from the monomer and octamer versions of (6). The two-dimensional nucleation model with octamer growth units follows the growth-rate trends very closely. The prediction from the monomer growth model progressively deviates from the measured growth

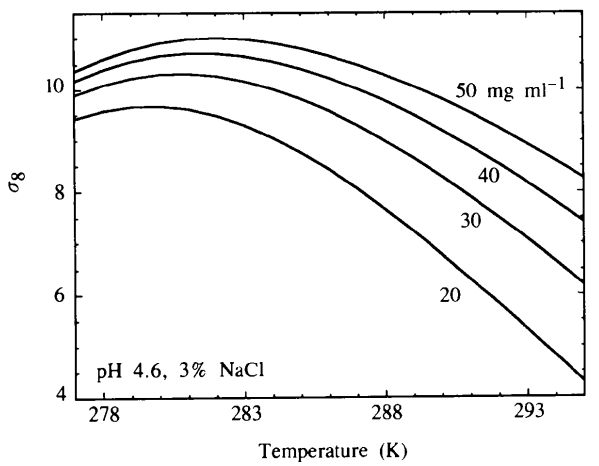

Fig. 11. Plots of the calculated octamer supersaturation σ_8 at various temperatures and lysozyme concentrations, for the pH 4.6/3% NaCl condition. The aggregate distributions were determined using the parameters in Table 1.

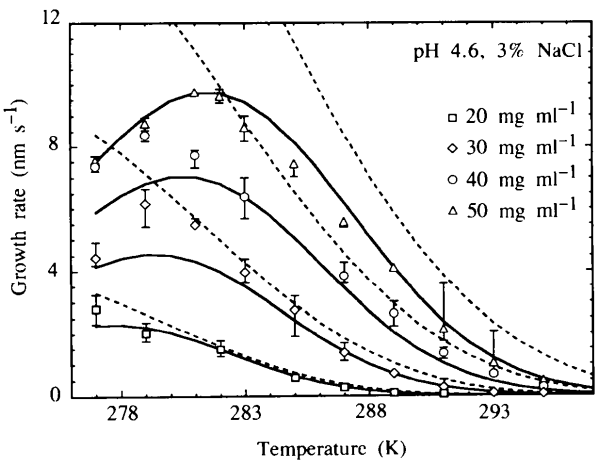

Fig. 12. Comparison of the measured (110) face growth rates of tetragonal lysozyme at pH 4.6/3% NaCl, with those predicted by the two-dimensional nucleation model in (6). The dashed lines show the predictions with monomer growth units from monodisperse solutions, while the solid lines show predictions with octamer growth units from polydisperse solutions.

rates with decreasing temperatures and increasing concentrations. Similar results were obtained with the other two data sets at pH 4.0, 5% NaCl and pH 5.0, 5% NaCl (not shown).

Although the above results seem to indicate that the growth of the (110) face proceeds by the addition of octamer units, in agreement with predictions from molecular packing considerations, this conclusion is based only on the averaged growth rates. Thus, growth on individual sites on the face may proceed by other growth units corresponding to the 4_3 helix, such as tetramers, hexamers and decamers, which when averaged may indicate octamer growth. This is particularly true of those aggregates not included in the sequence of aggregation reactions considered here, such as hexamers and decamers. However, the good agreements obtained for three different conditions and employing several growth mechanisms, suggests that octamers are at least the dominant unit for the (110) face.

6. Summary

In this study we have constructed the growth unit of (110) face of tetragonal lysozyme crystals from a crystallographic analysis, and compared its averaged growth rates with that predicted by several growth mechanisms. The main points can be summarized as follows.

(1) Crystallographic analysis of tetragonal lysozyme indicates that growth of the (110) face is a two-step process: the stronger intermolecular bonds cause the rapid formation and accumulation in the bulk solution of lysozyme aggregates corresponding to the 4_3 helix, while the weaker bonds are largely responsible for the slower attachment of the growth units to the crystal face.

(2) None of the standard growth-rate models tested here, with monomer growth units in a monodisperse lysozyme solution or with tetramer units in solutions with a distribution of aggregates, will explain the observed growth-rate trends with temperature and lysozyme concentration.

(3) Two dislocation and one two-dimensional nucleation growth-rate models with octamer growth units agree excellently with the measured growth-rate trends; this is in agreement with predictions from molecular packing considerations of tetragonal lysozyme crystals and observations from microscopic growth and etching studies.

(4) Even with the octamer units, the dislocation growth models tended to provide better predictions at the lower supersaturations and the two-dimensional nucleation model better predictions at the higher supersaturations as was shown to occur by microscopic studies; there was little to distinguish between the predictions by the two dislocation growth mechanisms.

This work was supported by grant NAG8-984 from the NASA/Marshall Space Flight Center and computer time provided by the Alabama Supercomputer Network.

References

Banerjee, S. K., Poglotti, A. & Rupley, J. A. (1975). *J. Biol. Chem.* **250**, 8260–8266.
Behlke, J. & Knespel, A. (1996). *J. Cryst. Growth*, **158**, 388–391.
Boistelle, R. & Astier, J. P. (1988). *J. Cryst. Growth*, **90**, 14–30.
Boué, F., Lefaucheux, F., Robert, M. C. & Rosenman, I. (1993). *J. Cryst. Growth*, **133**, 246–254.
Cacioppo, E. & Pusey, M. L. (1991). *J. Cryst. Growth*, **114**, 286–292.
Chernov, A. A. (1984). *Crystal Growth*. Berlin: Springer.
Chernov, A. A. (1988). *Contemp. Phys.* **30**, 251–276.
Diamond, R. (1974). *J. Mol. Biol.* **82**, 371–391.
Durbin, S. D. & Carlson, W. E. (1992). *J. Cryst. Growth*, **122**, 71–79.
Durbin, S. D. & Feher, G. (1990). *J. Mol. Biol.* **212**, 763–774.
Hampe, O. G., Tondo, C. V. & Hasson-Voloch, A. (1982). *Biophys. J.* **40**, 77–82.
International Tables for Crystallography (1983). Vol. A, No. 96. Dordrecht: Kluwer Academic Publishers.
Konnert, J. H., D'Antonio, P. & Ward, K. B. (1994). *Acta Cryst.* D**50**, 603–613.
Li, M., Nadarajah, A. & Pusey, M. L. (1995). *J. Cryst. Growth*, **156**, 121–132.
Minezaki, Y., Nimura, N., Ataka, M. & Katsura, T. (1996). *Biophys. Chem.* **58**, 355–363.
Monaco, L. A. & Rosenberger, F. (1993). *J. Cryst. Growth*, **129**, 465–484.
Nadarajah, A., Forsythe, E. L. & Pusey, M. L. (1995). *J. Cryst. Growth*, **151**, 163–172.
Nadarajah, A. & Pusey, M. L. (1996). *Acta Cryst.* D**52**, 983–996.
Pusey, M. L. (1991). *J. Cryst. Growth*, **110**, 60–65.
Sophianopoulos, A. J. (1969). *J. Biol. Chem.* **244**, 3188–3193.
Sophianopoulos, A. J. & Van Holde, K. E. (1964). *J. Biol. Chem.* **239**, 2516–2524.
Studebaker, J. F., Sykes, B. D. & Wien, R. (1971). *J. Am. Chem. Soc.* **93**, 4579–4585.
Vekilov, P. G., Ataka, M. & Katsura, T. (1995). *Acta Cryst.* D**51**, 207–219.
Vekilov, P. G. & Kuznetsov, Yu. G. (1992). *J. Cryst. Growth*, **119**, 248–260.
Vekilov. P. G. & Rosenberger, F. (1996). *J. Cryst. Growth*, **158**, 540–551.
Wilcox, F. H. & Daniel, L. J. (1954). *Arch. Biochem. Biophys.* **52**, 305–312.
Wilson, L. J., Adcock-Downey, L. & Pusey, M. L. (1996). *Biophys. J.* **71**, 2123–2129.
Zehavi, U. & Lustig, A. (1971). *Biochim. Biophys. Acta*, **236**, 127–130.